Detailed kinetic modeling of the formation of toxic polycyclic aromatic hydrocarbons (PAHs) coming from pyrolysis in low-pressure gas carburizing conditions

Tsilla Bensabath, Hubert Monnier, Pierre-Alexandre Glaude

Title: Detailed kinetic modeling of the formation of toxic polycyclic aromatic hydrocarbons (PAHs) coming from pyrolysis in low-pressure gas carburizing conditions

Authors:

Tsilla Bensabath[a,b] (tsilla.bensabath@univ-lorraine.fr)

Hubert Monnier[b] (hubert.monnier@inrs.fr)

Pierre-Alexandre Glaude[a] (pierre-alexandre.glaude@univ-lorraine.fr)

Affiliations:

[a]Laboratoire Réactions et Génie des Procédés, CNRS, Université de Lorraine, 1, rue Grandville, 54000 Nancy, France

[b]Institut National de Recherche et de Sécurité, 1, rue du Morvan, 54519 Vandœuvre-lès-Nancy, France

Abstract:

Hydrocarbon pyrolysis in low-pressure gas carburizing conditions leads to gas phase reactions, which produce polycyclic aromatic hydrocarbons (PAHs), some of which, such as benzo[*a*]pyrene, are carcinogenic. Workers can be exposed to these PAHs during maintenance and cleaning operations of carburizing furnaces. The aim of the study is the prediction of the formation of sixteen PAHs considered as priority pollutants by the Environmental Protection Agency in the United States (US EPA). A model has been implemented in order to describe the reaction pathways leading to their formation. It was validated using experimental data from the literature, obtained during pyrolysis of different hydrocarbons such as acetylene and ethylene. Flux analyses were realized in order to determine main reaction pathways leading to benzene depending on the reactant. Simulations were also performed to compare PAH formation between acetylene, ethylene and propane pyrolysis.

Keywords: PAHs; benzo[*a*]pyrene; low-pressure gas carburizing; kinetic model; hydrocarbon pyrolysis

1. Introduction

Low-pressure gas carburizing is a heat treatment process used to harden surface of steel by enriching the metal with carbon atoms coming from pyrolysis of hydrocarbons. This process is used to avoid wear of pieces subjected to strong constraints [1]. Unfortunately, in the same time, a wide variety of molecules and radicals are formed in the gas phase, which lead to the formation of polycyclic aromatic hydrocarbons (PAHs), which are soot precursors [2]. PAHs are toxic and some of them are known carcinogens [3]. This is the case of benzo[*a*]pyrene (B[*a*]P), which is used as a reference for assessing the carcinogenicity of other PAHs through the Toxic Equivalency Factor (TEF) [4]. Workers can be exposed to these substances by inhalation and skin contact during maintenance and cleaning operations of carburizing furnaces [5]. Sixteen PAHs, containing two to six carbon atom rings, have been classified as priority pollutants by the Environmental Protection Agency in the United States (EPA-PAHs) [6]. Understanding PAH formation is important to make safer and cleaner low-pressure gas carburizing processes, as other processes which can produce PAHs by hydrocarbon pyrolysis, such as atmosphere carburizing and carbonitriding, or by combustion.

There are two main pathways for the formation of the first aromatic rings, i.e. benzene and phenyl radical, which are the main actors of PAH growth [7,8]. The former, the $C_2 – C_4$ pathway, consists of the addition on an acetylene molecule of a C_4H_5 radical yielding benzene and of a C_4H_3 radical yielding a phenyl radical [9]. However, Miller and Melius estimated that this way cannot be the only responsible for the first ring formation [10]. They proposed the $C_3 – C_3$ pathway, which consists of the reaction between two propargyl radicals. Several studies focused on this reaction [11,12]. Cyclopentadienyl radicals also play an important role. They account for naphthalene formation by self-combination [13–15] and, in a similar way, in the formation of other PAHs such as phenanthrene [16].

Although the reactions which lead to the formation of benzene are well known today, the same cannot be said of the reactions responsible for the formation of heavier PAHs [8,17]. PAH growth results from various reaction pathways in competition. The best known is the Hydrogen Abstraction C_2H_2 Addition (HACA) mechanism presented by Frenklach et al. [18]. It consists in the elimination of a hydrogen atom from the initial PAH by an H-atom abstraction reaction, followed by the addition on the obtained radical site of an acetylene molecule. This mechanism is an important pathway because of

its low energy barrier and high exothermicity [19]. Other mechanisms were considered. Among them, there are the combinative growth mechanism, which consists in the growth of a PAH by adding aromatic rings, the cyclopentadienyl radical recombination [20] and the Hydrogen Abstraction Vinyl Addition (HAVA) mechanism [21]. Another possible pathway is the Diels-Alder mechanism but it is not competitive with the HACA mechanism [22].

Various models were developed in order to describe reactions, which occur during hydrocarbon combustion or pyrolysis up to the formation of PAHs. Frenklach et al. developed a model for acetylene and ethylene flames, which describes PAH growth up to molecules involving four aromatic rings and soot formation [7,23]. Slavinskaya et al. worked on a model for methane and ethylene flames and described PAH growth up to five aromatic rings [17,24]. Their model also allows an estimation of the amount of soot. Saggese et al. studied acetylene pyrolysis thanks to a model which combines a gas phase mechanism including PAH growth up to four aromatic rings and soot precursors with a soot formation mechanism [25]. More recently, Wang et al. published a model for propene pyrolysis [26] based on a model for ethane pyrolysis [27]. They did not describe the formation of heavy species (containing more than twelve carbon atoms) but emphasized the formation of first rings (benzene, styrene, naphthalene). In conditions close to low-pressure gas carburizing, Ziegler et al. proposed a model for Chemical Vapor Deposition (CVD) by propane pyrolysis, which takes into account PAH formation up to four aromatic rings [28,29]. The model which considers the heaviest PAHs is the model of Norinaga et al. It details PAH formation up to coronene, involving seven aromatic rings. It was validated for ethylene, acetylene and propylene pyrolysis in CVD conditions [30–32], as for propane pyrolysis [33]. Lastly, a model by Matsugi and Miyoshi [34], following studies of pyrolysis of mono-aromatics such as toluene [35,36], highlighted other reaction pathways to PAHs, such as the Phenyl Addition and Cyclization (PAC) mechanism.

This study aims to develop a model of hydrocarbon pyrolysis in gas carburizing conditions, i.e. at low pressure and at temperature ranging from 1173 to 1323 K [1,37], but without taking into account the presence of steel pieces. It focuses on the formation of the sixteen EPA-PAHs, which are not all modeled up to now in available mechanisms. These target PAHs are: naphthalene, acenaphthylene, acenaphthene, fluorene, phenanthrene, anthracene, fluoranthene, pyrene,

benzo[*a*]anthracene, chrysene, benzo[*b*]fluoranthene, benzo[*k*]fluoranthene, benzo[*a*]pyrene, indeno[1,2,3-*cd*]pyrene, dibenzo[*a*,*h*]anthracene and benzo[*ghi*]perylene. They are represented in Supplementary data (S1). The design of the model is detailed in section 2. Its validation was realized with experimental data from the literature.

Few experimental data on the sixteen EPA-PAHs in pyrolysis are available. Sánchez et al. quantified them at the outlet of a plug-flow reactor in the case of acetylene and ethylene pyrolysis [38–41]. They worked at different temperatures between 873 and 1323 K and at atmospheric pressure with a diluted reactant. At low pressure (undiluted reactant), Norinaga et al. measured thirteen EPA-PAHs during acetylene, ethylene and propylene pyrolysis in a plug-flow reactor at 1173 K [42]. Ziegler et al. pyrolysed propane in a perfectly stirred reactor at 2.7 kPa and at different temperatures between 1173 and 1323 K [28,29]. Only PAHs up to pyrene were experimentally quantified. All these data were used in the model development. In this study, simulations will be presented for acetylene and ethylene pyrolysis in the operating conditions of Norinaga et al. and of Sánchez et al.

2. Modeling

A detailed kinetic model for the pyrolysis of light hydrocarbons, such as acetylene, ethylene and propane, and PAH growth has been developed, based on a model for the combustion of aromatic compounds validated in particular in the case of combustion of ethylbenzene [43] and anisole [44]. The initial mechanism contained the reactions of pyrolysis and oxidation of many hydrocarbons, the reactions producing the first aromatic rings from lighter species by $C_2 – C_4$ pathway [45], $C_3 – C_3$ pathway [46] and cyclopentadienyl radicals [47], and the reactions of formation of PAHs up to four aromatic rings especially by the HACA mechanism [48]. Pressure dependence of rate constants is taken into account when available. This model has been simplified by removing all oxidation reactions and all species containing oxygen atoms. It has been completed with reactions for the production of heavier PAHs up to seven aromatic rings. Missing reactions have been added and some kinetic constants have been updated to take into account pathways, which could be negligible in oxidation conditions. The most important changes are detailed in this section. For all the reactions added, thermodynamic data of the compounds not present in the initial mechanism have been evaluated by the

85 software THERGAS [49] based on Benson's group additivity method or by analogy with isomers. The
86 final model contains 358 species and 1245 reactions. It is available in Supplementary data. In the
87 following, the observations about model predictions are made compared to the experimental data of
88 Norinaga and Deutschmann for acetylene and ethylene pyrolysis [31]. Species which appear in
89 reactions (R1) to (R20) are represented in Supplementary data (S2).
90
91 2.1. Reactant consumption and first steps of pyrolysis
92 Regarding acetylene pyrolysis, the model [44] overestimated the consumption of acetylene
93 (C_2H_2) as the production of vinylacetylene (C_4H_4), the main primary product of acetylene [50].
94 Reaction (R1), which was irreversible and thereby too fast, has been set reversible:

95 $$C_2H_2 + C_2H_2 \rightleftarrows C_4H_4 \qquad (R1)$$

96 Other reactions of vinylacetylene have been added:

97 $$C_4H_4 + C_2H_2 \rightleftarrows C_6H_6 \qquad (R2)$$

98 $$C_4H_4 + C_4H_4 \rightleftarrows C_8H_8 \qquad (R3)$$

99 $$C_4H_4 + C_4H_4 \rightleftarrows styrene \qquad (R4)$$

100 $$C_4H_4 + nC_4H_5 \rightleftarrows styrene + H \qquad (R5)$$

101 where C_6H_6, C_8H_8 and nC_4H_5 represent benzene, 1,3,5,7-cyclooctatetraene and 1,3-butadienyl radical,
102 respectively. Kinetic coefficients used for reactions (R2) and (R3) are those proposed by Norinaga et
103 al. [32] and those used for reactions (R4) and (R5) are from Slavinskaya and Frank [17]. Reactions of
104 consumption of 1,3,5,7-cyclooctatetraene have been added with kinetic coefficients proposed by
105 Dudek et al. [51]. They lead to the formation of benzene and styrene:

106 $$C_8H_8 \rightleftarrows C_6H_6 + C_2H_2 \qquad (R6)$$

107 $$C_8H_8 \rightleftarrows 1{,}5 - dihydropentalene \qquad (R7)$$

108 $$1{,}5 - dihydropentalene \rightleftarrows styrene \qquad (R8)$$

As to ethylene pyrolysis, the model underestimated the experimental consumption of ethylene (C_2H_4). A new pathway of consumption has been added with kinetic coefficients from Curran [52]:

$$C_2H_4 + C_2H_5 \rightleftarrows C_4H_9 \rightleftarrows C_4H_8 + H \qquad (R9)$$

where C_2H_5, C_4H_9 and C_4H_8 represent ethyl radical, butyl radical and 1-butene, respectively. Moreover, the reaction rate of the H-atom abstraction of ethylene by a hydrogen atom to produce a vinyl radical has a large influence on ethylene consumption. The rate constant of this reaction has therefore been updated with data of Wang and Frenklach [7].

2.2. Formation of first rings

The description of the evolution of first cyclic species containing five or six carbon atoms is essential because these rings are the basis of PAH formation. Some new reaction pathways for benzene and styrene formation have been presented in section 2.1 (reactions (R2) to (R8)). Reaction (R2) is an important reaction pathway for benzene formation in acetylene pyrolysis, especially at temperatures lower than 1200 K [25]. Flux analysis shows that reaction (R3) consumes more vinylacetylene than reaction (R4), even if this tendency is less pronounced when temperature increases. 1,3,5,7-cyclooctatetraene produced by (R3) is overwhelmingly converted through reaction (R6) to benzene, which is one of the main source of styrene. So, ultimately, both reactions (R3) and (R4) contribute to the formation of styrene during acetylene pyrolysis. When temperature increases, the part of reaction (R4) increases for short residence times (47% at 1073K and 54% at 1173K for τ = 0.24 s) but decreases for longer residence times (47% at 1073K and 28% at 1173K for τ = 1s).

Two other reaction pathways have been added to the model, leading to benzene and to cyclopentadiene, respectively. They come from a theoretical study of Cavallotti et al. [53] about reactions of 1,3-butadiene with vinyl radical (scheme S3). Kinetic coefficients are those proposed by these authors. The addition of these reactions is especially sensitive in prediction of 1,3-butadiene and benzene and thereby of most heavier aromatic compounds during ethylene pyrolysis.

A reaction pathway to indene (C_9H_8) from cyclopentadienyl radical (C_5H_5) via benzyl radical (C_7H_7) by successive additions of acetylene molecules has also been added. Several studies on this

pathway exist in the literature even if the intermediate C_7H_7 is not necessarily benzyl radical [54–56]. Two reactions, (R10) and (R11), have been set reversible and updated:

$$C_7H_7 \rightleftarrows C_5H_5 + C_2H_2 \qquad (R10)$$

$$C_9H_8 + H \rightleftarrows C_7H_7 + C_2H_2 \qquad (R11)$$

Kinetic coefficients of reaction (R11) have been modified based on the theoretical study of Kislov and Mebel [57]. This study details the intermediate elementary reactions included in this pathway with their rate constant. We obtained global rate constants (Equations (E1) and (E2)) by the quasi-steady-state assumption (QSSA):

$$k_{R11,d} = 1200\, T^{0.072} exp\left(-\frac{27600}{RT}\right) \qquad (E1)$$

$$k_{R11,r} = 6910\, T^{-1.863} exp\left(\frac{4250}{RT}\right) \qquad (E2)$$

with direct constant $k_{R11,d}$ and reverse constant $k_{R11,r}$ in $cm^3mol^{-1}s^{-1}$, temperature T in K and gas constant R in cal $mol^{-1}K^{-1}$. This pathway is sensitive on indene amount, especially reaction (-R10) producing benzyl: the addition of benzyl radical on acetylene also produces indene via an intermediate radical (C_6H_5–CH_2–CH=CH). About 70% of benzyl comes from reaction (-R10). Similarly to cyclopentadiene, indene is an important intermediate in PAH growth. It is a precursor of heavy compounds as, for example, cyclopentadiene produces naphthalene [16].

2.3. Formation of PAHs

Among the sixteen EPA-PAHs, six which include two to four rings were already present in the model: naphthalene, acenaphthylene, phenanthrene, anthracene, pyrene and chrysene. Nine have been added with their formation reactions coming from Norinaga et al.'s model [32]: acenaphthene, fluorene, fluoranthene, benzo[*a*]anthracene, benzo[*b*]fluoranthene, benzo[*k*]fluoranthene, benzo[*a*]pyrene, indeno[1,2,3-*cd*]pyrene and benzo[*ghi*]perylene. The formation and the consumption of these species involve a significant number of other species whose inclusion in the model has been necessary. Among them, there are a lot of radical species and other PAHs like acephenanthrylene,

benzo[*e*]pyrene, perylene, anthanthrene or coronene. Eventually, the sixteenth EPA-PAH is dibenzo[*a*,*h*]anthracene. To our knowledge, there is no model in the literature, which describes pathways leading to it. Reactions have been written based on those producing benzo[*a*]anthracene, with the same kinetic coefficients. Reactions implying dibenzo[*a*,*h*]anthracene or radicals, which derive from it, are reported in Table 1. Figure 1 shows the species involved with their corresponding notations. Dibenzo[*a*,*h*]anthracene can be produced via different pathways:

- from phenanthrene directly, by addition with phenylacetylene or derived radicals (Reactions 1 and 2 in Table 1).
- from benzo[*a*]anthracene, by the HACA mechanism or by addition of derived radicals with vinylacetylene (Reactions 3 to 6).
- by combination of species with a five-membered ring, such as benzo[*e*]indenyl radical with indenyl radical (Reactions 7 and 8).

From this point, missing reaction pathways have been added to improve the simulation of the amount of several PAHs, which were significantly underestimated.

In Norinaga et al [32], phenanthrene formation can occur through combination of two benzyl radicals. These reactions have been included in the model. By analogy, pathways to chrysene and benzo[*a*]anthracene formation have been written from the combination of a benzyl radical with a 1-naphthylmethyl radical for chrysene and a 2-naphthylmethyl radical for benzo[*a*]anthracene. These new pathways are presented in Supplementary data (S4) in the case of benzo[*a*]anthracene formation.

Other reactions from the literature have been integrated in order to complete the possible reaction pathways of the following PAHs:

- naphthalene [24]:

phenyl + 1,3-butadiene → naphthalene + H_2 + H (R12)

- acenaphthylene [17]:

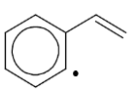

+ diacetylene → acenaphthylene + H (R13)

- chrysene [32]:

indenyl + indenyl → chrysene + 2 H (R14)

- pyrene [24]:

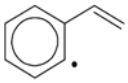 + phenylacetylene → pyrene + H_2 + H (R15)

 → pyrene + 2 H (R16)

- benzo[*ghi*]fluoranthene [17]:

indenyl + indenyl → benzo[*ghi*]fluoranthene + 2 H_2 (R17)

- benzo[*a*]pyrene [24]:

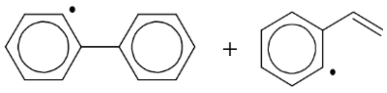 → benzo[*a*]pyrene + 2 H_2 (R18)

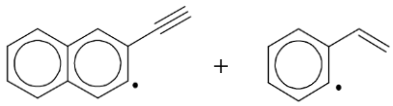 → benzo[*a*]pyrene + 2 H (R19)

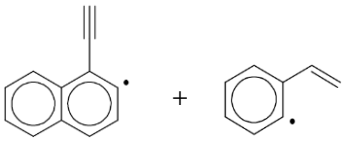 → benzo[*a*]pyrene + 2 H (R20)

Note that these reactions are not elementary steps but a lumping of successive reactions, and are therefore irreversible.

2.4. Influence of acetone

Because of the presence of acetone in acetylene bottles to avoid self-detonation, five reactions of the decomposition of acetone have been included in the mechanism. They come from the model of Norinaga and Deutschmann [31]. Despite the low amount of this impurity, acetone is very reactive and it dominates radical initiation during acetylene pyrolysis in our operating conditions, especially by methyl radical formation [58].

3. Model validation

The validation of the model was realized thanks to various experimental data available in the literature. In this section, the simulations were obtained in the operating conditions of Norinaga and Deutschmann [31] at low pressure and in those of Sánchez et al. [38,39] at atmospheric pressure for acetylene and ethylene pyrolysis in a plug-flow reactor. Simulations were performed using the PSR (Perfectly Stirred Reactor model) module in the Chemkin software suite. The plug-flow reactor was modeled as a succession of continuous stirred-tank reactors. A series of fifty PSRs were used in order to obtain solutions independent of the number of elementary reactors. Error factors in section 3.1 have been calculated for the experimental point available at the longest residence time.

3.1. Low-pressure pyrolysis - Comparison with Norinaga and Deutschmann results

3.1.1. Acetylene pyrolysis

The inlet stream of the reactor is composed of 98% acetylene, 0.2% methane and 1.8% acetone. Figures 2, 3 and 4 compare simulations with experimental points [31]. Simulations in the same conditions with the model of Norinaga et al. [32] are also represented. Graphs present the evolution of mole fractions of the different species plotted as a function of the residence time into the reactor. Figure 2 shows results for light species, i.e. the consumption of acetylene and the formation of hydrogen, methane, ethylene, vinylacetylene and propyne, at 1173 K and 8 kPa. Figure 3 shows the profiles of benzene, toluene, styrene, indene, naphthalene and acenaphthylene at 1173 K and 8 kPa. Eventually, the formation of heavier PAHs at 1173 K and 15 kPa is presented in Figure 4. Some EPA-PAHs were not quantified experimentally. They are treated in section 3.2. Regarding experiments, material balances show that more than 90% carbon is generally analyzed at the outlet [42]. The estimated uncertainties for concentrations range between ±9% and ±32%, increasing with the molecular weight of molecules [31].

Simulation agrees with experimental points for acetylene, vinylacetylene and propyne. Hydrogen and methane are underestimated (by a factor 1.8) and ethylene is overestimated (by a factor 3). Regarding first aromatic rings, benzene and styrene, which are the major aromatic species quantified experimentally, are fairly well represented by the model. The main primary product of

acetylene pyrolysis is vinylacetylene, which mostly leads to benzene and styrene formation. For these compounds, our simulations better represent experimental points than the model of Norinaga et al. (especially for vinylacetylene). Meanwhile, ethylene is overpredicted. Flux analysis, detailed in Supplementary data (S5), shows that it is produced from vinylacetylene by decomposition into vinyl radical, which leads to ethylene, but also by decomposition of phenylethyl radical, which comes from styrene. Styrene is mainly produced from benzene. In the model, added reactions of vinylacetylene lead to the formation of benzene and styrene (reactions (R2) to (R8)), and so, to the formation of ethylene. In this way, the overprediction of ethylene is related to the much better representation of vinylacetylene compared to Norinaga's model, but ethylene plays a less important role in aromatic formation [31]. Therefore, the first steps of the pyrolysis are correctly described by the model. Tendencies of toluene and indene are not well represented. They reach a maximum for a short residence time while experimental points present a monotonic growth on the range of studied residence times. These two species are correlated by reaction (R11), discussed in section 2.2.

In a general way, simulation reproduces well the order of magnitude of PAH mole fractions. Compared to the model of Norinaga et al., our model gives results closer to experimental data for most PAHs. Some compounds like naphthalene, acenaphthylene and benzo[*k*]fluoranthene are fairly well represented. However, some other profiles have a convex shape while experimental curves have a concave shape. Phenanthrene is overestimated (by a factor 2.4) while anthracene is underestimated (by a factor 3). These two species are linked in the model: higher amounts of anthracene leads to higher amounts of phenanthrene and vice versa. Flux analysis shows that the main pathway for anthracene formation is the isomerization of phenanthrene, which is also the most sensitive reaction on anthracene formation. However, increasing the kinetic constant of this reversible reaction (which comes from Marinov et al. [59]) by a factor 10 has almost no effect on concentration, whereas the sensitivity coefficient of the reaction drops off. The equilibrium constant of the reaction of isomerization is then more sensitive: decreasing the enthalpy of formation of anthracene by 4 kcal mol^{-1} permits to fit the mole fraction of this species in acetylene pyrolysis conditions. However, the enthalpy of formation used in the model for anthracene and phenanthrene are from Kudchadker et al.[60], i.e. 55.0 kcal mol^{-1} and 49.5 kcal mol^{-1}, respectively. These data are in very good agreement with the review of Roux et al.

[61] (54.8±0.7 kcal mol^{-1} and 48.3±0.6 kcal mol^{-1} respectively). A larger spread between enthalpies of formation of both isomers would be far beyond the range of uncertainty. Note that the main pathway for phenanthrene formation is the addition of a radical derived from phenylacetylene on benzene. This pathway cannot lead to the formation of anthracene but another important pathway for anthracene formation can be missing. Benzo[*ghi*]perylene is significantly underestimated (by a factor 21), even if its mole fraction is the lowest among quantified PAHs. Some formation pathways should still be missing. It is produced by the HACA mechanism from benzo[*e*]pyrene and perylene and consumed to produce coronene. Another pathway could be the addition of aromatic rings on lighter PAHs such as phenanthrene.

3.1.2. Ethylene pyrolysis

The inlet stream of the reactor is composed of 99.4% ethylene, 0.2% methane and 0.4% ethane. Figures 5 and 6 show the evolution of mole fractions of light species and of first aromatic rings and light PAHs respectively, plotted as a function of the residence time, at 1173 K and 8 kPa. Figure 7 shows profiles of heavy EPA-PAHs for which experimental points [31] exist at 1173 K and 15 kPa. As in the case of acetylene pyrolysis, simulations with the model of Norinaga et al. [32] are presented for comparison.

Ethylene consumption is well represented by the model as well as hydrogen, acetylene and vinylacetylene profiles overall. Methane production is underestimated (by a factor 1.8) and 1,3-butadiene is overestimated (by a factor 2) although the curve correctly represents its tendency. Regarding first aromatic rings, the model well describes benzene evolution. Profiles are fairly well respected so it is possible to consider that the model correctly represents the first steps of ethylene pyrolysis despite differences observed for toluene and styrene as well as for indene from some residence time (compounds in much smaller amounts than benzene). The link between toluene and indene was mentioned in section 3.1.1. The validation of the model for the formation of light species is confirmed by the good agreement of simulation results with experimental data for light PAHs, namely naphthalene, acenaphthylene and phenanthrene. Anthracene is underestimated (by a factor 13).

290 Generally, tendencies and orders of magnitude of heavier PAHs are fairly well represented.
291 However, the model underestimates pyrene formation (by a factor 8.2) and overestimates chrysene and
292 benzo[*a*]anthracene formation (by a factor 1.8 and 2.4 respectively). A flux analysis shows that the
293 main reaction pathways of formation of these four-ring compounds differ between ethylene pyrolysis
294 and acetylene pyrolysis. In the case of ethylene, chrysene and benzo[*a*]anthracene are mainly produced
295 (at 91% and 87% respectively for a residence time of 1 s) by combination of two indenyl radicals
296 which come from indene. These pathways may be too fast. It could explain chrysene and
297 benzo[*a*]anthracene overestimation along with indene underestimation for large residence times. As to
298 pyrene, the formation pathway by addition of a styryl radical on phenylacetylene which is important
299 during acetylene pyrolysis (46% for a residence time of 1 s) is negligible during ethylene pyrolysis
300 (1.7% for a residence time of 1 s). The underestimation of styrene by the simulation can cause this
301 change. So, improving styrene profile might allow to enhance pyrene formation. Otherwise, the model
302 reproduces benzo[*a*]pyrene evolution very well but it underestimates fluoranthene and
303 benzo[*k*]fluoranthene formation (by a factor 12 and 14, respectively).
304 Our simulations give much better results than those of Norinaga et al. for benzene, light PAHs
305 (naphthalene, acenaphthylene and phenanthrene) and benzo[*a*]pyrene but they are worse for some
306 heavier PAHs. Nevertheless, naphthalene, which experimental fraction is up to 100 times higher than
307 that of other PAHs, is very well predicted here, while Norinaga's model overestimates it by a factor of
308 4. Since naphthalene is one of the base compounds in PAH enlargement, this explain partly the present
309 fluoranthene and benzo[*k*]fluoranthene underestimation. A flux analysis shows that fluoranthene
310 mainly comes (at 67% for a residence time of 1 s) from the addition of a phenyl radical on naphthalene
311 or of a naphthyl radical on benzene. As to benzo[*k*]fluoranthene, it is formed by the addition of a
312 naphthyl radical on naphthalene.
313
314 3.2. Atmospheric pyrolysis - Comparison with Sánchez et al. results
315 Sánchez et al. quantified the sixteen EPA-PAHs during acetylene and ethylene pyrolysis under
316 various conditions of temperature [38,39,41], residence time [41] and concentration [39]. They worked
317 at atmospheric pressure, leading to soot formation despite the low fraction of hydrocarbon (3%)

diluted in nitrogen. It makes the comparison with the model difficult because the model does not include soot formation. Moreover, pressure changes kinetics of some reactions.

Simulations were realized at 1173 K and atmospheric pressure for a residence time of 1.45 s. The inlet stream of the reactor is composed of 3% reactant (acetylene or ethylene) and 97% inert (nitrogen), which corresponds to a partial pressure of 3 kPa for the reactant. Temperature of 1173 K has been chosen to make easier the comparison with experimental data: at a lower temperature, too few PAHs are formed and at a higher temperature, soot formation becomes important.

Absolute simulated amounts of each PAH are much lower than experimental results except for naphthalene during ethylene pyrolysis. The authors give a carbon yield of light compounds (from H_2 to C_8) [38,39] and it seems that the model overestimates these light compounds while it underestimates PAHs. In particular, available data on benzene during acetylene pyrolysis [39] show that this compound is overestimated in simulations. All of this suggests that PAH formation from light species and first aromatic rings is too slow in these conditions and that the influence of the pressure is not well taken into account in the model. Nevertheless, without more detailed experimental data on light compounds, it is not possible to make conclusive hypotheses. A quantitative comparison between experiments and simulations results cannot be performed. Following observations are qualitative.

In both experiments and simulations, acetylene pyrolysis produces larger amounts of all PAHs than ethylene pyrolysis, except for acenaphthene. In a general way, predicted relative amounts of PAHs, compared one to another, agree with experiments. Experimentally, the predominant PAHs are the lightest up to pyrene except for acenaphthene, which is formed in small amount. This result is found by simulation but with some differences. On one hand, anthracene is predicted in too small amount. On the other hand, in ethylene pyrolysis, benzo[*a*]anthracene and chrysene are predicted in larger amounts than pyrene. These elements are consistent with the observations made at low pressure and discussed in section 3.1.

About PAHs which were not quantified by Norinaga et al., simulations seem to lead to correct orders of magnitude for fluorene, benzo[*b*]fluoranthene and dibenzo[*a*,*h*]anthracene compared to other PAHs. Acenaphthene is predicted in too small amount during acetylene pyrolysis but is well represented during ethylene pyrolysis. It can be explain by the fact that acenaphthene is

overwhelmingly produced in the model by the addition of an 1-naphthyl radical on ethylene. Alternative pathways may take place during acetylene pyrolysis. This makes consistent the predominance of acenaphthene during ethylene pyrolysis at 1173 K, i.e. at lower temperature than what is experimentally observed. Indeno[1,2,3-*cd*]pyrene seems underestimated compared to other PAHs. Some formation pathways for this compound must be missing in the model. For now, it is only produced from pyrene by addition of benzene or phenyl and from benzo[*b*]fluoranthene by the HACA mechanism. Benzo[*ghi*]perylene seems also underestimated during ethylene pyrolysis as during acetylene pyrolysis. Its formation pathways were already discussed in section 3.1.1.

4. Discussion

4.1. Reaction pathways of benzene production

It is essential to predict accurately benzene evolution because it is one of the main precursors of PAHs. Moreover, it plays a major role in their growth thanks to the combinative growth mechanism. In section 1, the main pathways of formation of benzene described in the literature were recalled, but the model takes into account many other pathways. A flux analysis was realized in order to determine the origin of benzene in the case of pyrolysis of different hydrocarbons. Simulations were performed at 1173 K, 8 kPa and a reactant conversion of approximately 40%. This conversion corresponds to a residence time of 1 s for acetylene and ethylene, a residence time of 0.22 s for propylene and a residence time of 0.003 s for propane. In each case, reactant is considered pure. Figure 8 details the main pathways of the formation of benzene during acetylene and ethylene pyrolysis.

Regarding acetylene pyrolysis, benzene mainly comes from the addition reaction of vinylacetylene with acetylene molecules (R2) or with vinyl radicals (R21):

$$C_4H_4 + C_2H_3 \rightleftarrows C_6H_6 + H \qquad (R21)$$

Vinylacetylene is largely formed by addition of two acetylene molecules, either directly (R1) or via diacetylene and iC_4H_3 radical ($HC \equiv C - C = CH_2$).

During ethylene pyrolysis, two major reaction pathways, which are roughly equivalent, appear. Both involve 1,3-butadiene, one of the major product, mainly formed by the addition of vinyl radical on an ethylene molecule:

$$C_2H_4 + C_2H_3 \rightleftarrows 1,3 - C_4H_6 + H \qquad (R22)$$

The first pathway is the cyclization of a linear C_6H_9 radical (CH2=CH−CH2−CH=CH−CH2), which is produced by the addition of vinyl radical on 1,3-butadiene. The second involves fulvene, which undergoes an isomerization to benzene. Fulvene is mainly formed from iC_4H_5 radical (H_2C=CH−C=CH_2) by the following reaction:

$$iC_4H_5 + C_2H_2 \rightleftarrows fulvene + H \qquad (R23)$$

iC_4H_5 radical is produced by H-atom abstractions on 1,3-butadiene.

Lastly, the model was used to simulate propylene pyrolysis and propane pyrolysis. Reaction pathways to benzene are similar in both cases. Benzene comes mainly from fulvene isomerization. However, unlike ethylene pyrolysis, fulvene is formed from propylene thanks to a reaction chain involving different C_3 species. These reactions are the following:

- formation of tC_3H_5 radical (H_2C=C−CH_3) from propylene by H-atom abstraction
- formation of allene by β-scission of tC_3H_5 radical
- formation of propargyl radical C_3H_3 from allene by H-atom abstraction
- combination of a propargyl radical with an allyl radical or with another propargyl radical to form fulvene. Allyl radicals are derived from propylene by H-atom abstraction.

In the case of propane pyrolysis, H-atom abstraction reactions of propane lead to iC_3H_7 radical (H_3C−CH−CH_3), which produces propylene by β-scission.

The different reaction pathways to benzene, which have been detailed here, represent the major pathways for the different reactants. Nevertheless, minor pathways involve other cyclic species such as methylcyclopentadiene, toluene, styrene or 1,3,5,7-cyclooctatetraene.

4.2. Influence of the reactant on the formation of PAHs

The model was used to compare PAH formation during the pyrolysis of three different hydrocarbons: acetylene, ethylene and propane. These reactants were chosen because they are the compounds most used in low-pressure gas carburizing [37] and because they represent an alkyne, an alkene and an alkane, respectively.

As an order of magnitude, Figure 9 presents mole fractions for each of the sixteen EPA-PAHs produced by the pyrolysis of the three pure reactants at 1173 K, 15 kPa and at a reactant conversion of 50%. This conversion is equivalent to a residence time of 0.68 s for acetylene, 1.05 s for ethylene and 3.9 10^{-3} s for propane. Propane conversion is much faster than acetylene or ethylene conversion because of fast reactions of C-C bond breaking [62]. To better understand the results, a flux analysis for benzo[*a*]pyrene formation is presented in Figure 10. It shows the pathways of formation of benzo[*a*]pyrene during acetylene and ethylene pyrolysis. Propane pyrolysis is not represented on the figure but pathways are similar to those for ethylene: benzo[*a*]pyrene is produced from benzo[*a*]anthracene at 26% and from chrysene at 70% (via intermediate radicals); benzo[*a*]anthracene and chrysene are formed from the recombination of two indenyl radicals at 98% and 99% respectively. Figure 9 shows that all PAHs are present in larger amounts during acetylene pyrolysis than during ethylene pyrolysis, which joins the results of section 3. This is explained by the importance of the HACA mechanism in the process of PAH growth, which can be noticed in Figure 10. Benzo[*a*]pyrene is almost entirely produced through this mechanism from benzo[*a*]anthracene and chrysene. These two PAHs are produced by combination of two indenyl radicals during ethylene pyrolysis but they are mainly produced from naphthyl radicals or naphthalene during acetylene pyrolysis. Pathways for naphthalene formation are presented in Supplementary data (S6). They show that the HACA mechanism is mostly responsible for the production of naphthalene during acetylene pyrolysis. Otherwise, Figure 9 shows that for propane pyrolysis, PAHs are formed in much lower amounts, especially for the heaviest. Alkanes are less favorable to the formation of aromatic rings because C/H ratio is smaller than for alkenes or alkynes. It is therefore necessary to produce unsaturated products to allow cyclisation and aromatic formation. Moreover, because of the weakness of C-C bonds, propane pyrolysis generates many radicals. These radicals have to lead first to the formation of unsaturated molecules (acetylene, ethylene), which then allow PAH formation.

However, these results are obtained for the same conversion rate but for different residence times. In industrial gas carburizing, residence time into the reactor is an important parameter because it has an influence on the amount of carbon adsorbed on steel. Figure 11 represents the evolution of the mole fraction of benzo[*a*]pyrene plotted as a function of the residence time for acetylene, ethylene and propane pyrolysis at 1173 K and 15 kPa. On the one hand, benzo[*a*]pyrene is always more produced by acetylene than ethylene. On the other hand, this PAH is more produced by propane than acetylene or ethylene at low residence times because of fast conversion of propane. Propane conversion is stabilized very quickly since it reaches 99% at 0.04 s while acetylene and ethylene conversion gradually increases. From 0.4 s, propane produces less benzo[*a*]pyrene than acetylene (converted at 38%) and from 0.98 s, it produces less benzo[*a*]pyrene than ethylene (converted at 49%). Other PAHs have a similar trend. A sensitivity analysis was carried out at a residence time of 1 s and 1173 K to highlight the reactions which impact the production of benzo[*a*]pyrene. It is available in Supplementary data (S7). During acetylene, ethylene and propane pyrolysis, the kinetically limiting reaction for benzo[*a*]pyrene is the addition of a radical derived from benzo[*a*]anthracene on acetylene to form benzo[*a*]pyrene. This strengthens the previous observations on the importance of the HACA mechanism. Other sensitive reactions during acetylene pyrolysis are those of formation and consumption of iC_4H_3 radical, which is an important intermediate of benzene formation (Figure 8). During ethylene and propane pyrolysis, sensitive reactions on benzo[*a*]pyrene involve chrysene and derived radicals, and benzyl radical which is an important intermediate of indene formation (Supplementary data (S6)). Similarities between ethylene and propane are understandable because ethylene is the main primary product of propane pyrolysis.

Acetylene produces more PAHs than propane from some residence time but it is also one of the most efficient hydrocarbons for surface reactions [63]. By making the approximation that only acetylene is adsorbed on steel, the time required for carburizing depends on the amount of acetylene available in gas phase, more important for acetylene pyrolysis than for propane pyrolysis. By dividing mole fractions of PAHs for a residence time of 1 s by the mole fraction of acetylene present at this time, several PAHs are formed in larger amount for propane than for acetylene, including benzo[*a*]pyrene. These results are presented in Figure 12 for the sixteen EPA-PAHs.

5. Conclusion

A detailed kinetic model has been developed to describe the formation of PAHs from light hydrocarbon pyrolysis (acetylene, ethylene, etc.). It is mainly focused on the formation of the sixteen EPA-PAHs at low pressure. The aim is to use the model to evaluate the potential of toxicity, especially linked to benzo[*a*]pyrene concentration, of processes such as low-pressure gas carburizing. It was validated by various experimental data from the literature. Compared to previous model, it includes new reaction pathways from the literature and represents an improvement for the reactions of small unsaturated species and for the formation of first rings. However, some differences with experimental points are observed, which shows that some reaction pathways are still missing or wrongly evaluated.

Simulations allowed to highlight the diversity of reaction pathways leading to benzene and to show the strong dependence between reactant and the predominance of some pathways compared to others. They also allowed to compare PAH formation during the pyrolysis of different hydrocarbons.

Experiments of acetylene, ethylene and propane pyrolysis will be performed in the near future in a plug-flow reactor and in a perfectly stirred reactor. They will allow a better validation of the model in low-pressure gas carburizing conditions. Some experiments will be carried out with an iron piece to study the influence of surface reactions on PAH formation and to determine how it is possible to insert those reactions in the model.

Supplementary data

Mechanism and transport data in CHEMKIN format, and Supplementary data associated with this article can be found in the online version.

References

[1] K. Yada, O. Watanabe, Reactive flow simulation of vacuum carburizing by acetylene gas, Comput. Fluids. 79 (2013) 65–76. doi:10.1016/j.compfluid.2013.03.005.

[2] H. Richter, J.B. Howard, Formation of polycyclic aromatic hydrocarbons and their growth to soot—a review of chemical reaction pathways, Prog. Energy Combust. Sci. 26 (2000) 565–608.

[3] K. Straif, R. Baan, Y. Grosse, B. Secretan, F. El Ghissassi, V. Cogliano, Carcinogenicity of polycyclic aromatic hydrocarbons, Lancet Oncol. 6 (2005) 931–932. doi:10.1016/S1470-2045(05)70458-7.

[4] I. Nisbet, P. Lagoy, Toxic Equivalency Factors (TEFs) for Polycyclic Aromatic Hydrocarbons (PAHs), Regul. Toxicol. Pharmacol. 16 (1992) 290–300. doi:10.1016/0273-2300(92)90009-X.

[5] C. Champmartin, F. Jeandel, H. Monnier, Maintenance of Low-Pressure Carburizing Furnaces: A Source of PAH Exposure, Ann. Occup. Hyg. (2016).
[6] N.E. Sánchez, A. Callejas, J. Salafranca, Á. Millera, R. Bilbao, M.U. Alzueta, Formation and characterization of polyaromatic hydrocarbons, in: Clean. Combust. - Dev. Detail. Chem. Kinet. Models, 2013: pp. 283–302.
[7] H. Wang, M. Frenklach, A detailed kinetic modeling study of aromatics formation in laminar premixed acetylene and ethylene flames, Combust. Flame. 110 (1997) 173–221.
[8] H.A. Gueniche, J. Biet, P.A. Glaude, R. Fournet, F. Battin-Leclerc, A comparative study of the formation of aromatics in rich methane flames doped by unsaturated compounds, Fuel. 88 (2009) 1388–1393. doi:10.1016/j.fuel.2009.03.006.
[9] P.R. Westmoreland, A.M. Dean, J.B. Howard, J.P. Longwell, Forming benzene in flames by chemically activated isomerization, J. Phys. Chem. 93 (1989) 8171–8180. doi:10.1021/j100362a008.
[10] J.A. Miller, C.F. Melius, Kinetic and thermodynamic issues in the formation of aromatic compounds in flames of aliphatic fuels, Combust. Flame. 91 (1992) 21–39. doi:10.1016/0010-2180(92)90124-8.
[11] J.A. Miller, S.J. Klippenstein, The Recombination of Propargyl Radicals and Other Reactions on a C6H6 Potential, J. Phys. Chem. A. 107 (2003) 7783–7799. doi:10.1021/jp030375h.
[12] R.X. Fernandes, H. Hippler, M. Olzmann, Determination of the rate coefficient for the C3H3 + C3H3 reaction at high temperatures by shock-tube investigations, Proc. Combust. Inst. 30 (2005) 1033–1038. doi:10.1016/j.proci.2004.08.204.
[13] C.F. Melius, M.E. Colvin, N.M. Marinov, W.J. Pitz, S.M. Senkan, Reaction mechanisms in aromatic hydrocarbon formation involving the C5H5 cyclopentadienyl moiety, Symp. Int. Combust. 26 (1996) 685–692. doi:10.1016/S0082-0784(96)80276-1.
[14] A.M. Mebel, V.V. Kislov, Can the C5H5 + C5H5 → C10H10 → C10H9 + H/C10H8 + H2 Reaction Produce Naphthalene? An Ab Initio/RRKM Study, J. Phys. Chem. A. 113 (2009) 9825–9833. doi:10.1021/jp905931j.
[15] C. Cavallotti, D. Polino, On the kinetics of the C5H5 + C5H5 reaction, Proc. Combust. Inst. 34 (2013) 557–564. doi:10.1016/j.proci.2012.05.097.
[16] N.M. Marinov, W.J. Pitz, C.K. Westbrook, A.M. Vincitore, M.J. Castaldi, S.M. Senkan, C.F. Melius, Aromatic and Polycyclic Aromatic Hydrocarbon Formation in a Laminar Premixed n-Butane Flame, Combust. Flame. 114 (1998) 192–213. doi:10.1016/S0010-2180(97)00275-7.
[17] N.A. Slavinskaya, P. Frank, A modelling study of aromatic soot precursors formation in laminar methane and ethene flames, Combust. Flame. 156 (2009) 1705–1722. doi:10.1016/j.combustflame.2009.04.013.
[18] M. Frenklach, D.W. Clary, W.C. Gardiner Jr., S.E. Stein, Detailed kinetic modeling of soot formation in shock-tube pyrolysis of acetylene, Symp. Int. Combust. 20 (1984) 887–901. doi:10.1016/S0082-0784(85)80578-6.
[19] V.V. Kislov, A.I. Sadovnikov, A.M. Mebel, Formation Mechanism of Polycyclic Aromatic Hydrocarbons beyond the Second Aromatic Ring, J. Phys. Chem. A. 117 (2013) 4794–4816. doi:10.1021/jp402481y.
[20] H. Böhm, H. Jander, PAH formation in acetylene–benzene pyrolysis, Phys. Chem. Chem. Phys. 1 (1999) 3775–3781.
[21] B. Shukla, M. Koshi, A novel route for PAH growth in HACA based mechanisms, Combust. Flame. 159 (2012) 3589–3596. doi:10.1016/j.combustflame.2012.08.007.
[22] V.V. Kislov, N.I. Islamova, A.M. Kolker, S.H. Lin, A.M. Mebel, Hydrogen Abstraction Acetylene Addition and Diels−Alder Mechanisms of PAH Formation: A Detailed Study Using First Principles Calculations, J. Chem. Theory Comput. 1 (2005) 908–924. doi:10.1021/ct0500491.
[23] J. Appel, H. Bockhorn, M. Frenklach, Kinetic modeling of soot formation with detailed chemistry and physics: laminar premixed flames of C2 hydrocarbons, Combust. Flame. 121 (2000) 122–136. doi:10.1016/S0010-2180(99)00135-2.

[24] V. Chernov, M.J. Thomson, S.B. Dworkin, N.A. Slavinskaya, U. Riedel, Soot formation with C1 and C2 fuels using an improved chemical mechanism for PAH growth, Combust. Flame. 161 (2014) 592–601. doi:10.1016/j.combustflame.2013.09.017.
[25] C. Saggese, N.E. Sánchez, A. Frassoldati, A. Cuoci, T. Faravelli, M.U. Alzueta, E. Ranzi, Kinetic Modeling Study of Polycyclic Aromatic Hydrocarbons and Soot Formation in Acetylene Pyrolysis, Energy Fuels. 28 (2014) 1489–1501. doi:10.1021/ef402048q.
[26] K. Wang, S.M. Villano, A.M. Dean, Fundamentally-based kinetic model for propene pyrolysis, Combust. Flame. 162 (2015) 4456–4470. doi:10.1016/j.combustflame.2015.08.012.
[27] C. Xu, A.S. Al Shoaibi, C. Wang, H.-H. Carstensen, A.M. Dean, Kinetic Modeling of Ethane Pyrolysis at High Conversion, J. Phys. Chem. A. 115 (2011) 10470–10490. doi:10.1021/jp206503d.
[28] I. Ziegler, R. Fournet, P.M. Marquaire, Pyrolysis of propane for CVI of pyrocarbon: Part I. Experimental and modeling study of the formation of toluene and aliphatic species, J. Anal. Appl. Pyrolysis. 73 (2005) 212–230. doi:10.1016/j.jaap.2004.12.005.
[29] I. Ziegler, R. Fournet, P.-M. Marquaire, Pyrolysis of propane for CVI of pyrocarbon: Part II. Experimental and modeling study of polyaromatic species, J. Anal. Appl. Pyrolysis. 73 (2005) 231–247. doi:10.1016/j.jaap.2005.03.007.
[30] K. Norinaga, O. Deutschmann, Proc.EUROCVD-15, (2005). http://www.detchem.com/ (accessed June 24, 2014).
[31] K. Norinaga, O. Deutschmann, Detailed kinetic modeling of gas-phase reactions in the chemical vapor deposition of carbon from light hydrocarbons, Ind. Eng. Chem. Res. 46 (2007) 3547–3557.
[32] K. Norinaga, O. Deutschmann, N. Saegusa, J. Hayashi, Analysis of pyrolysis products from light hydrocarbons and kinetic modeling for growth of polycyclic aromatic hydrocarbons with detailed chemistry, J. Anal. Appl. Pyrolysis. 86 (2009) 148–160. doi:10.1016/j.jaap.2009.05.001.
[33] R.U. Khan, S. Bajohr, D. Buchholz, R. Reimert, H.D. Minh, K. Norinaga, V.M. Janardhanan, S. Tischer, O. Deutschmann, Pyrolysis of propane under vacuum carburizing conditions: An experimental and modeling study, J. Anal. Appl. Pyrolysis. 81 (2008) 148–156. doi:10.1016/j.jaap.2007.09.012.
[34] A. Matsugi, A. Miyoshi, Modeling of two- and three-ring aromatics formation in the pyrolysis of toluene, Proc. Combust. Inst. 34 (2013) 269–277. doi:10.1016/j.proci.2012.06.032.
[35] B. Shukla, A. Susa, A. Miyoshi, M. Koshi, In Situ Direct Sampling Mass Spectrometric Study on Formation of Polycyclic Aromatic Hydrocarbons in Toluene Pyrolysis, J. Phys. Chem. A. 111 (2007) 8308–8324. doi:10.1021/jp071813d.
[36] B. Shukla, A. Susa, A. Miyoshi, M. Koshi, Role of Phenyl Radicals in the Growth of Polycyclic Aromatic Hydrocarbons, J. Phys. Chem. A. 112 (2008) 2362–2369. doi:10.1021/jp7098398.
[37] D. Buchholz, R.U. Khan, S. Bajohr, R. Reimert, Computational Fluid Dynamics Modeling of Acetylene Pyrolysis for Vacuum Carburizing of Steel, Ind. Eng. Chem. Res. 49 (2010) 1130–1137. doi:10.1021/ie900996h.
[38] N.E. Sánchez, A. Callejas, Á. Millera, R. Bilbao, M.U. Alzueta, Polycyclic Aromatic Hydrocarbon (PAH) and Soot Formation in the Pyrolysis of Acetylene and Ethylene: Effect of the Reaction Temperature, Energy Fuels. 26 (2012) 4823–4829. doi:10.1021/ef300749q.
[39] N.E. Sánchez, Á. Millera, R. Bilbao, M.U. Alzueta, Polycyclic aromatic hydrocarbons (PAH), soot and light gases formed in the pyrolysis of acetylene at different temperatures: Effect of fuel concentration, J. Anal. Appl. Pyrolysis. 103 (2013) 126–133. doi:10.1016/j.jaap.2012.10.027.
[40] N.E. Sánchez, J. Salafranca, A. Callejas, Á. Millera, R. Bilbao, M.U. Alzueta, Quantification of polycyclic aromatic hydrocarbons (PAHs) found in gas and particle phases from pyrolytic processes using gas chromatography–mass spectrometry (GC–MS), Fuel. 107 (2013) 246–253. doi:10.1016/j.fuel.2013.01.065.
[41] N.E. Sánchez, A. Callejas, A. Millera, R. Bilbao, M.U. Alzueta, Formation of PAH and soot during acetylene pyrolysis at different gas residence times and reaction temperatures, Energy. 43 (2012) 30–36. doi:10.1016/j.energy.2011.12.009.

[42] K. Norinaga, O. Deutschmann, K.J. Hüttinger, Analysis of gas phase compounds in chemical vapor deposition of carbon from light hydrocarbons, Carbon. 44 (2006) 1790–1800. doi:10.1016/j.carbon.2005.12.050.
[43] B. Husson, M. Ferrari, O. Herbinet, S.S. Ahmed, P.-A. Glaude, F. Battin-Leclerc, New experimental evidence and modeling study of the ethylbenzene oxidation, Proc. Combust. Inst. 34 (2013) 325–333. doi:10.1016/j.proci.2012.06.002.
[44] M. Nowakowska, O. Herbinet, A. Dufour, P.-A. Glaude, Detailed kinetic study of anisole pyrolysis and oxidation to understand tar formation during biomass combustion and gasification, Combust. Flame. 161 (2014) 1474–1488. doi:10.1016/j.combustflame.2013.11.024.
[45] H.A. Gueniche, P.A. Glaude, R. Fournet, F. Battin-Leclerc, Rich premixed laminar methane flames doped by light unsaturated hydrocarbons: II. 1,3-Butadiene, Combust. Flame. 151 (2007) 245–261. doi:10.1016/j.combustflame.2007.05.007.
[46] H.A. Gueniche, P.A. Glaude, G. Dayma, R. Fournet, F. Battin-Leclerc, Rich methane premixed laminar flames doped with light unsaturated hydrocarbons: I. Allene and propyne, Combust. Flame. 146 (2006) 620–634. doi:10.1016/j.combustflame.2006.07.004.
[47] H.A. Gueniche, P.A. Glaude, R. Fournet, F. Battin-Leclerc, Rich methane premixed laminar flames doped by light unsaturated hydrocarbons: III. Cyclopentene, Combust. Flame. 152 (2008) 245–261. doi:10.1016/j.combustflame.2007.07.012.
[48] N.A. Slavinskaya, U. Riedel, S.B. Dworkin, M.J. Thomson, Detailed numerical modeling of PAH formation and growth in non-premixed ethylene and ethane flames, Combust. Flame. 159 (2012) 979–995. doi:10.1016/j.combustflame.2011.10.005.
[49] C. Muller, V. Michel, G. Scacchi, G. Côme, Thergas - a Computer-Program for the Evaluation of Thermochemical Data of molecules and free-radicals in the gas phase, J. Chim. Phys. Phys.-Chim. Biol. 92 (1995) 1154–1178.
[50] O.A. Rokstad, O.A. Lindvaag, A. Holmen, Acetylene Pyrolysis in Tubular Reactor, Int. J. Chem. Kinet. 46 (2014) 104–115. doi:10.1002/kin.20830.
[51] D. Dudek, K. Glänzer, J. Troe, Pyrolysis of 1.3.5.7-Cyclooctatetraene, Semibullvalene, and 1.5-Dihydropentalene in Shock Waves and in a Flow System (Part I), Berichte Bunsen-Ges.-Phys. Chem. Chem. Phys. 83 (1979) 776–788.
[52] H.J. Curran, Rate constant estimation for C1 to C4 alkyl and alkoxyl radical decomposition, Int. J. Chem. Kinet. 38 (2006) 250–275. doi:10.1002/kin.20153.
[53] C. Cavallotti, S. Fascella, R. Rota, S. Carrà, A Quantum Chemistry Study of the Formation of Pah and Soot Precursors Through Butadiene Reactions, Combust. Sci. Technol. 176 (2004) 705–720. doi:10.1080/00102200490428026.
[54] V.D. Knyazev, I.R. Slagle, Kinetics of the Reaction between Propargyl Radical and Acetylene, J. Phys. Chem. A. 106 (2002) 5613–5617. doi:10.1021/jp0144909.
[55] C. Cavallotti, S. Mancarella, R. Rota, S. Carra, Conversion of C5 into C6 cyclic species through the formation of C7 intermediates, J. Phys. Chem. A. 111 (2007) 3959–3969. doi:10.1021/jp067117f.
[56] J.D. Savee, T.M. Selby, O. Welz, C.A. Taatjes, D.L. Osborn, Time- and Isomer-Resolved Measurements of Sequential Addition of Acetylene to the Propargyl Radical, J. Phys. Chem. Lett. 6 (2015) 4153–4158. doi:10.1021/acs.jpclett.5b01896.
[57] V.V. Kislov, A.M. Mebel, Ab Initio G3-type/Statistical Theory Study of the Formation of Indene in Combustion Flames. I. Pathways Involving Benzene and Phenyl Radical, J. Phys. Chem. A. 111 (2007) 3922–3931. doi:10.1021/jp067135x.
[58] M.B. Colket III, D.J. Seery, H.B. Palmer, The pyrolysis of acetylene initiated by acetone, Combust. Flame. 75 (1989) 343–366. doi:10.1016/0010-2180(89)90048-5.
[59] N.M. Marinov, W.J. Pitz, C.K. Westbrook, M.J. Castaldi, S.M. Senkan, Modeling of Aromatic and Polycyclic Aromatic Hydrocarbon Formation in Premixed Methane and Ethane Flames, Combust. Sci. Technol. 116–117 (1996) 211–287. doi:10.1080/00102209608935550.

635 [60] S.A. Kudchadker, A.P. Kudchadker, B.J. Zwolinski, Chemical thermodynamic properties of
636 anthracene and phenanthrene, J. Chem. Thermodyn. 11 (1979) 1051–1059. doi:10.1016/0021-
637 9614(79)90135-6.
638 [61] M.V. Roux, M. Temprado, J.S. Chickos, Y. Nagano, Critically Evaluated Thermochemical
639 Properties of Polycyclic Aromatic Hydrocarbons, J. Phys. Chem. Ref. Data. 37 (2008) 1855–1996.
640 doi:10.1063/1.2955570.
641 [62] Y.-R. Luo, Handbook of Bond Dissociation Energies in Organic Compounds, CRC Press, 2003.
642 [63] R. Lacroix, R. Fournet, I. Ziegler-Devin, P.-M. Marquaire, Kinetic modeling of surface reactions
643 involved in CVI of pyrocarbon obtained by propane pyrolysis, Carbon. 48 (2010) 132–144.
644 doi:10.1016/j.carbon.2009.08.041.

Table

Table 1: Reactions of production and consumption of dibenzo[*a*,*h*]anthracene (DBAHA3L) and derived radicals with kinetic constants[1] by analogy with benzo[*a*]anthracene reactions

No.	Reaction[2]	A ($cm^3mol^{-1}s^{-1}$)	n	Ea ($cal\ mol^{-1}$)
1	$phenanthrene + C_6H_4\#C_2H \bullet\leftrightarrow DBAHA3L + H$	$8.51\ 10^{11}$	0	3 987
2	$phenanthrene - 2 + C_6H_5\#C_2H \leftrightarrow DBAHA3L + H$	$8.51\ 10^{11}$	0	3 987
3	$BAA3L - 9 + C_4H_4 \leftrightarrow DBAHA3L + H$	$9.90\ 10^{30}$	5.07	21 101
4	$BAA3L - 8 + C_4H_4 \leftrightarrow DBAHA3L + H$	$9.90\ 10^{30}$	5.07	21 101
5	$BAA3LE - 1P + C_2H_2 \leftrightarrow DBAHA3L - 1$	$1.87\ 10^{7}$	1.787	3 262
6	$BAA3LE - 2S + C_2H_2 \leftrightarrow DBAHA3L - 12$	$1.87\ 10^{7}$	1.787	3 262
7	$BEindene \bullet + indenyl \rightarrow DBAHA3L + H + H$	$1.00\ 10^{12}$	0	7 999
8	$NFindene \bullet + C_5H_5 \rightarrow DBAHA3L + H + H$	$1.00\ 10^{12}$	0	7 999
9	$DBAHA3L + H \leftrightarrow DBAHA3L - 1 + H_2$	$3.23\ 10^{7}$	2.095	15 843
10	$DBAHA3L + H \leftrightarrow DBAHA3L - 12 + H_2$	$3.23\ 10^{7}$	2.095	15 843
11	$DBAHA3L + H \leftrightarrow DBAHA3L - 4 + H_2$	$3.23\ 10^{9}$	2.095	15 843
12	$DBAHA3L - 1 + H \leftrightarrow DBAHA3L$	$5.00\ 10^{13}$	0	0
13	$DBAHA3L - 12 + H \leftrightarrow DBAHA3L$	$5.00\ 10^{13}$	0	0
14	$DBAHA3L - 4 + H \leftrightarrow DBAHA3L$	$5.00\ 10^{13}$	0	0
15	$DBAHA3L + CH_3 \leftrightarrow DBAHA3L - 1 + CH_4$	$2.00\ 10^{12}$	0	15 059
16	$DBAHA3L + CH_3 \leftrightarrow DBAHA3L - 12 + CH_4$	$2.00\ 10^{12}$	0	15 059
17	$DBAHA3L + C_2H_3 \leftrightarrow DBAHA3L - 1 + C_2H_4$	$6.00\ 10^{11}$	0	12 978
18	$DBAHA3L + C_2H_3 \leftrightarrow DBAHA3L - 12 + C_2H_4$	$6.00\ 10^{11}$	0	12 978

[1] $k = AT^n exp(-Ea/RT)$ with gas constant R in $cal\ mol^{-1}K^{-1}$

[2] Notations used for the different species are clarified in Figure 1

Figure captions

Figure 1: Molecules and radicals involved in Table 1

Figure 2: Mole fraction profiles of light species during acetylene pyrolysis at 1173 K and 8 kPa. Points refer to experiments [31], solid lines to simulations and dashed lines to the model of Norinaga et al. [32].

Figure 3: Mole fraction profiles of first aromatic rings and light PAHs during acetylene pyrolysis at 1173 K and 8 kPa. Points refer to experiments [31], solid lines to simulations and dashed lines to the model of Norinaga et al. [32].

Figure 4: Mole fraction profiles of heavy PAHs during acetylene pyrolysis at 1173 K and 15 kPa. Points refer to experiments [31], solid lines to simulations and dashed lines to the model of Norinaga et al. [32]. * indicates a logarithmic scale in ordinate.

Figure 5: Mole fraction profiles of light species during ethylene pyrolysis at 1173 K and 8 kPa. Points refer to experiments [31], solid lines to simulations and dashed lines to the model of Norinaga et al. [32].

Figure 6: Mole fraction profiles of first aromatic rings and light PAHs during ethylene pyrolysis at 1173 K and 8 kPa. Points refer to experiments [31], solid lines to simulations and dashed lines to the model of Norinaga et al. [32].

Figure 7: Mole fraction profiles of heavy PAHs during ethylene pyrolysis at 1173 K and 15 kPa. Points refer to experiments [31], solid lines to simulations and dashed lines to the model of Norinaga et al. [32]. * indicates a logarithmic scale in ordinate.

Figure 8: Main reaction pathways for benzene formation at 1173 K, 8 kPa and 1 s of residence time during: a) acetylene pyrolysis; b) ethylene pyrolysis. Percentages are related to the weight of the reaction in the formation of products.

Figure 9: Mole fractions of the EPA-PAHs obtained by modeling during acetylene, ethylene and propane pyrolysis at 1173 K, 15 kPa and a reactant conversion of 50%

Figure 10: Main reaction pathways for benzo[a]pyrene formation at 1173 K, 15 kPa and a reactant conversion of 50% during acetylene pyrolysis (percentages in bold) and ethylene pyrolysis (percentages in italic). Percentages are related to the weight of the reaction in the formation of products. Reaction pathways for naphthalene and indene formation are available in Supplementary data (S6).

Figure 11: Profiles of benzo[*a*]pyrene mole fraction obtained by modeling during acetylene, ethylene and propane pyrolysis at 1173 K and 15 kPa

Figure 12: Mole fractions of the EPA-PAHs divided by the mole fraction of acetylene obtained by modeling during acetylene and propane pyrolysis at 1173 K, 15 kPa and a residence time of 1 s

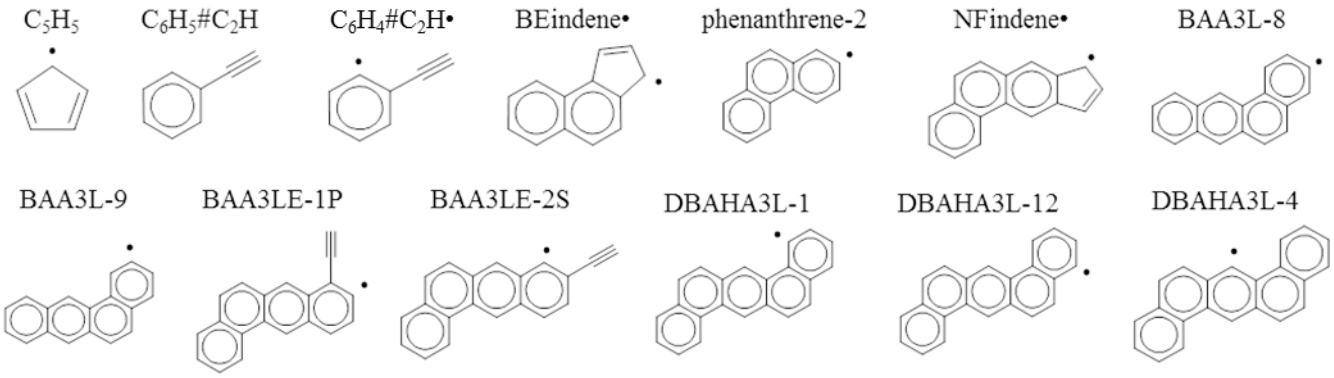

Figure 1: Molecules and radicals involved in Table 1

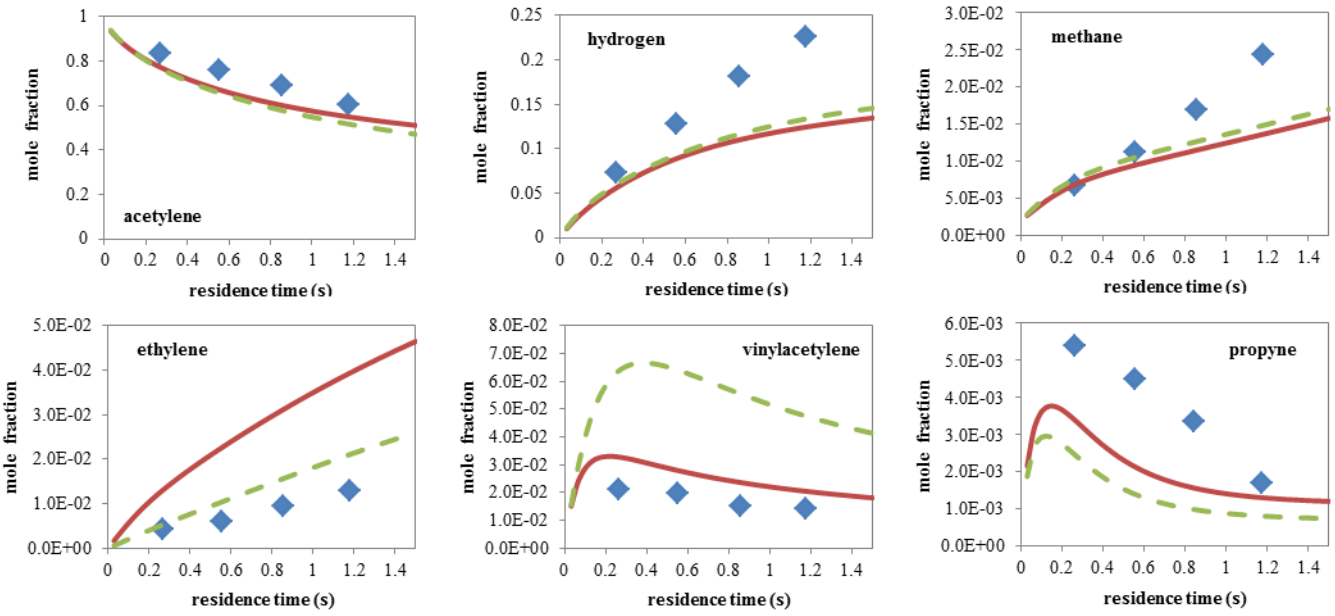

Figure 2: Mole fraction profiles of light species during acetylene pyrolysis at 1173 K and 8 kPa. Points refer to experiments [31], solid lines to simulations and dashed lines to the model of Norinaga et al. [32].

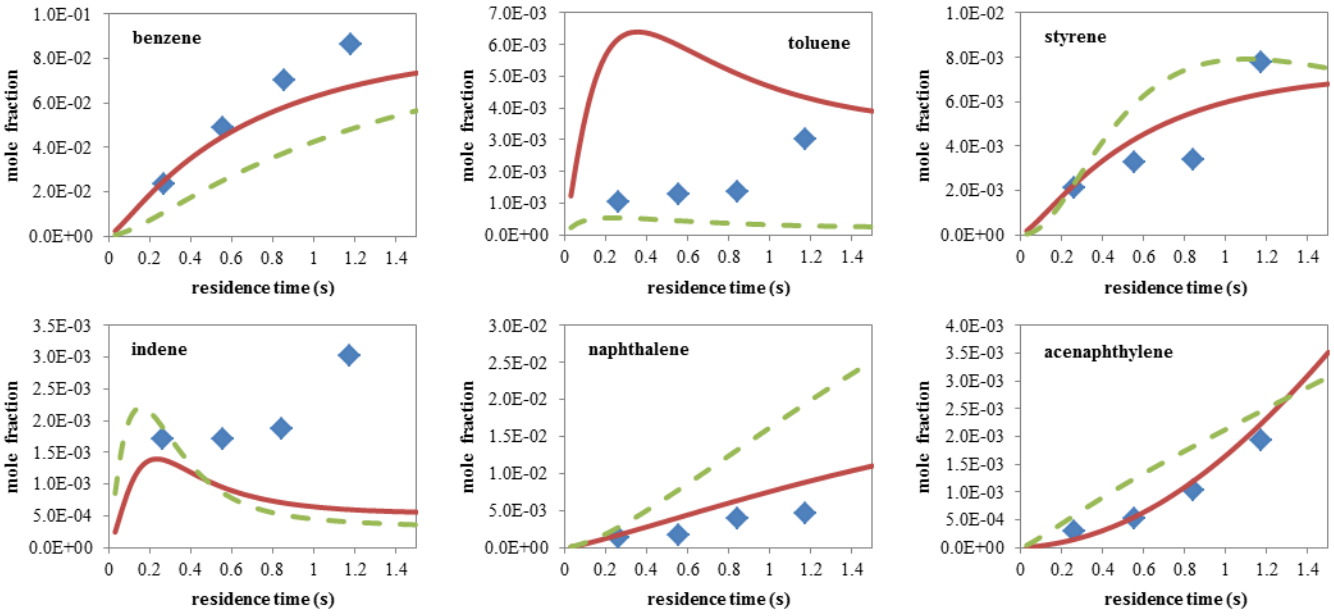

Figure 3: Mole fraction profiles of first aromatic rings and light PAHs during acetylene pyrolysis at 1173 K and 8 kPa. Points refer to experiments [31], solid lines to simulations and dashed lines to the model of Norinaga et al. [32].

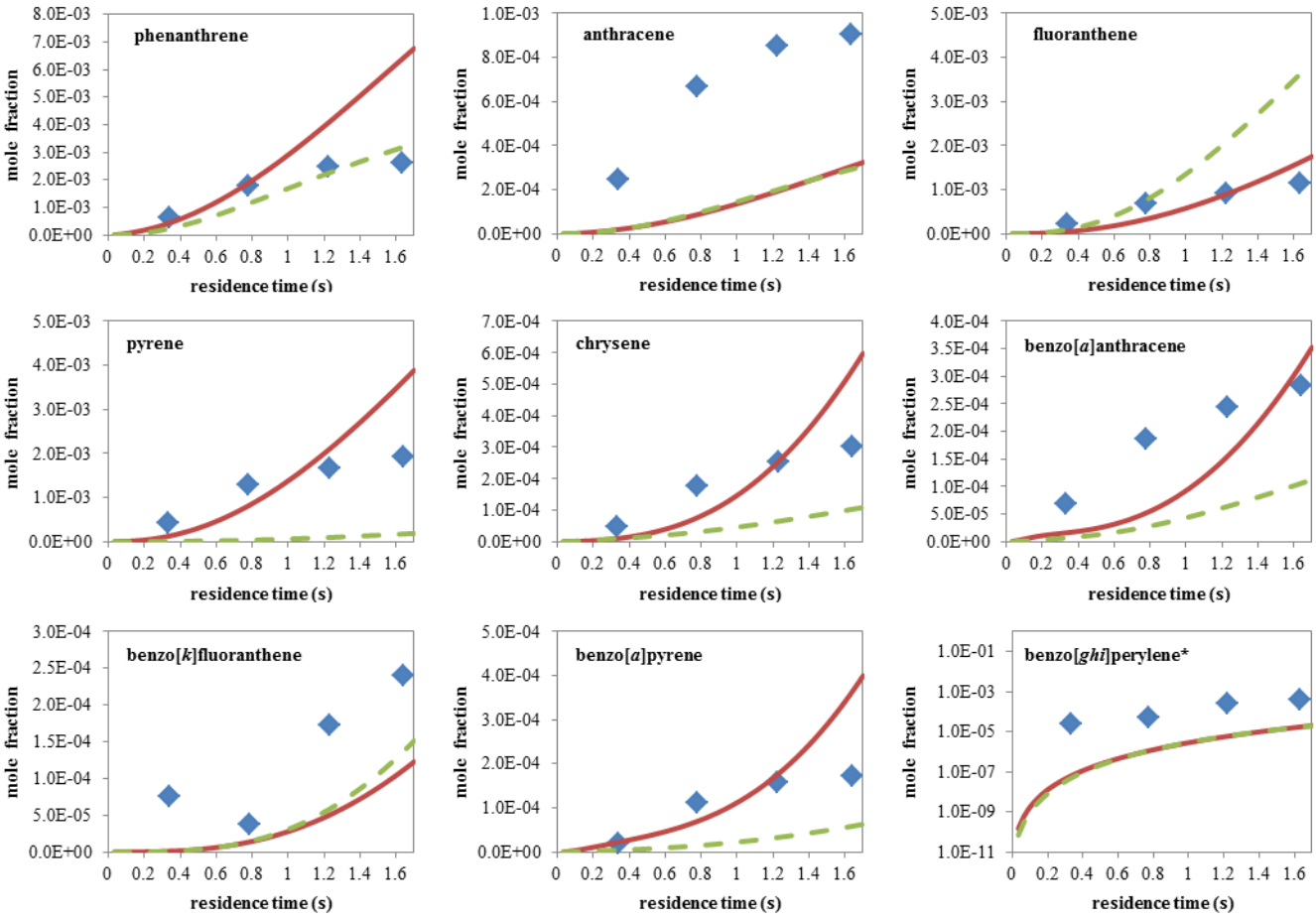

Figure 4: Mole fraction profiles of heavy PAHs during acetylene pyrolysis at 1173 K and 15 kPa. Points refer to experiments [31], solid lines to simulations and dashed lines to the model of Norinaga et al. [32]. * indicates a logarithmic scale in ordinate.

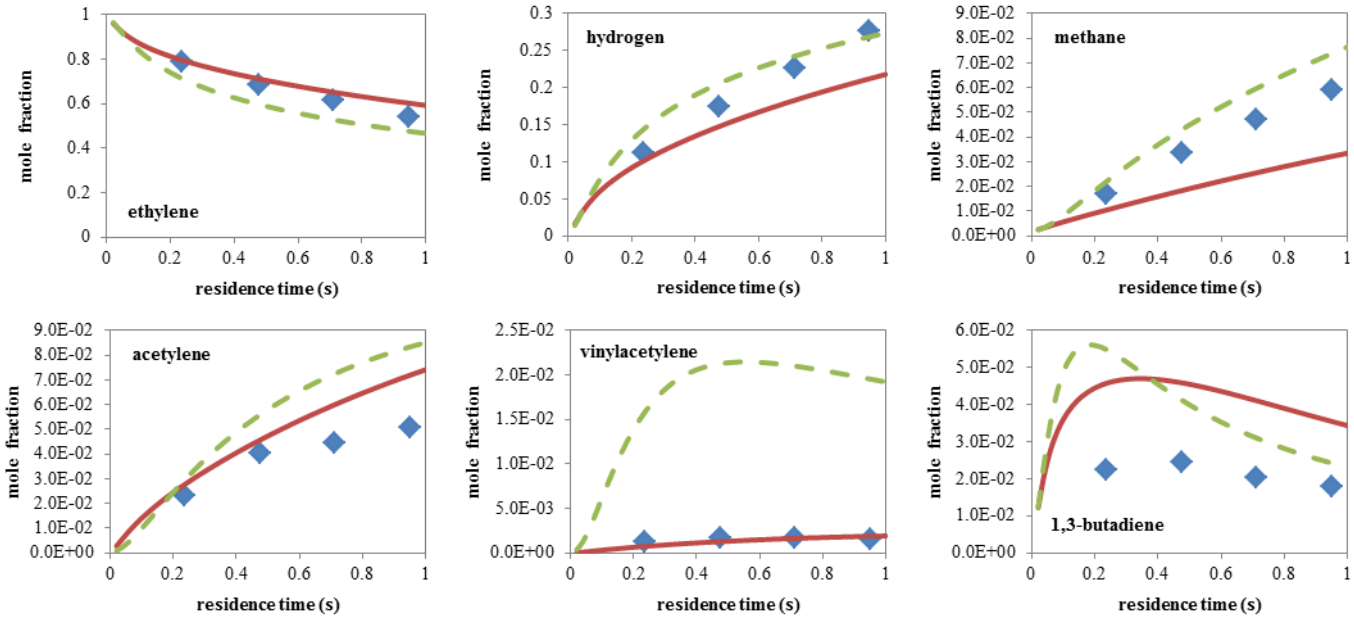

Figure 5: Mole fraction profiles of light species during ethylene pyrolysis at 1173 K and 8 kPa. Points refer to experiments [31], solid lines to simulations and dashed lines to the model of Norinaga et al. [32].

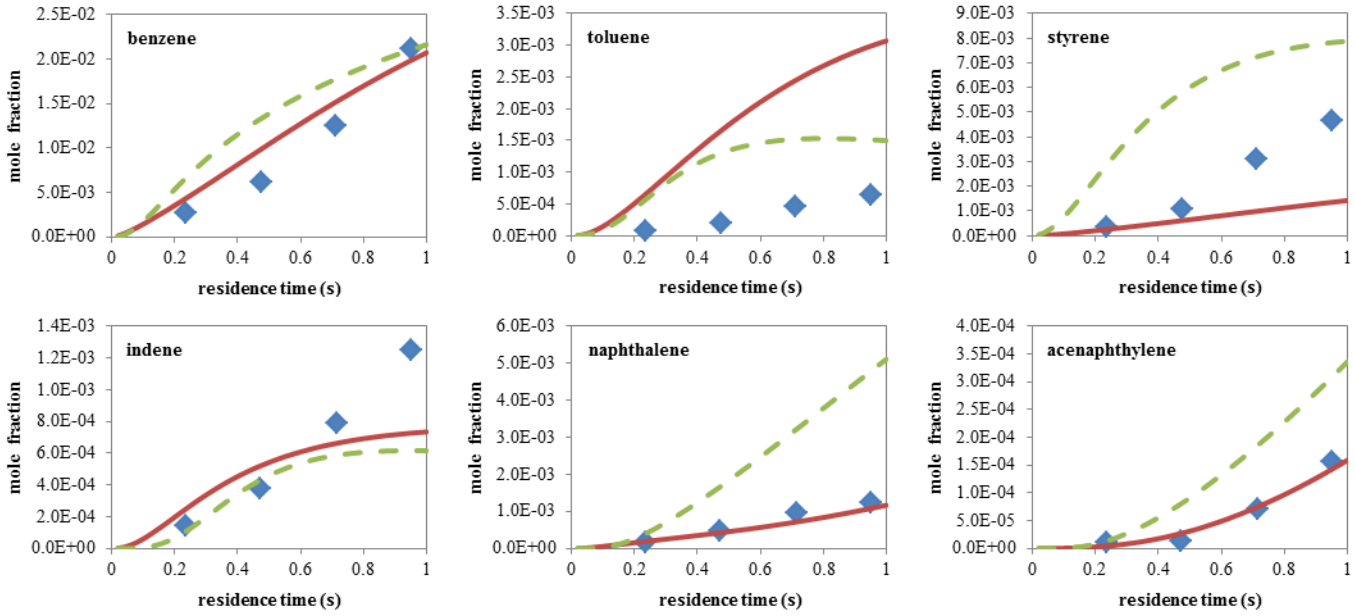

Figure 6: Mole fraction profiles of first aromatic rings and light PAHs during ethylene pyrolysis at 1173 K and 8 kPa. Points refer to experiments [31], solid lines to simulations and dashed lines to the model of Norinaga et al. [32].

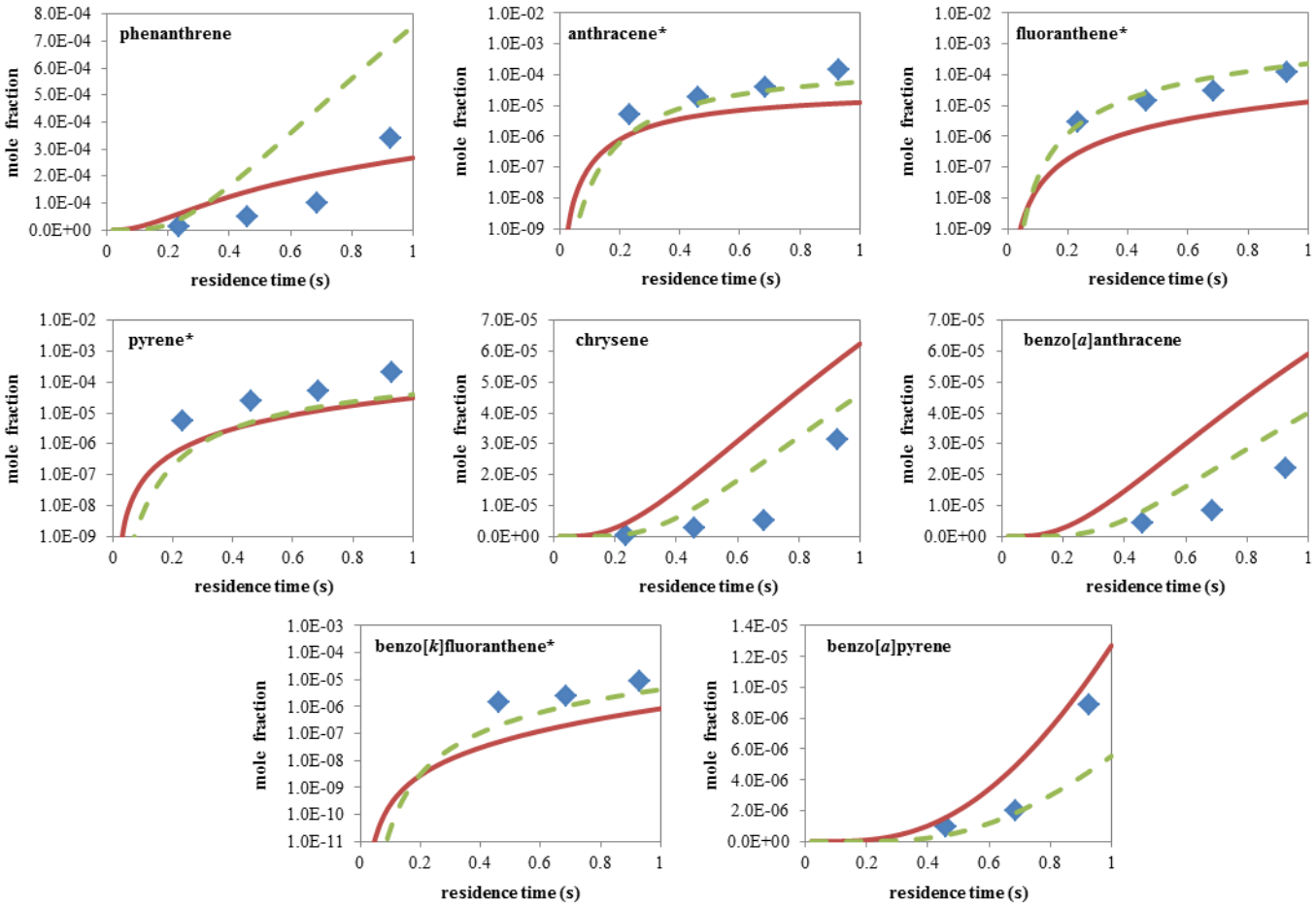

Figure 7: Mole fraction profiles of heavy PAHs during ethylene pyrolysis at 1173 K and 15 kPa. Points refer to experiments [31], solid lines to simulations and dashed lines to the model of Norinaga et al. [32]. * indicates a logarithmic scale in ordinate.

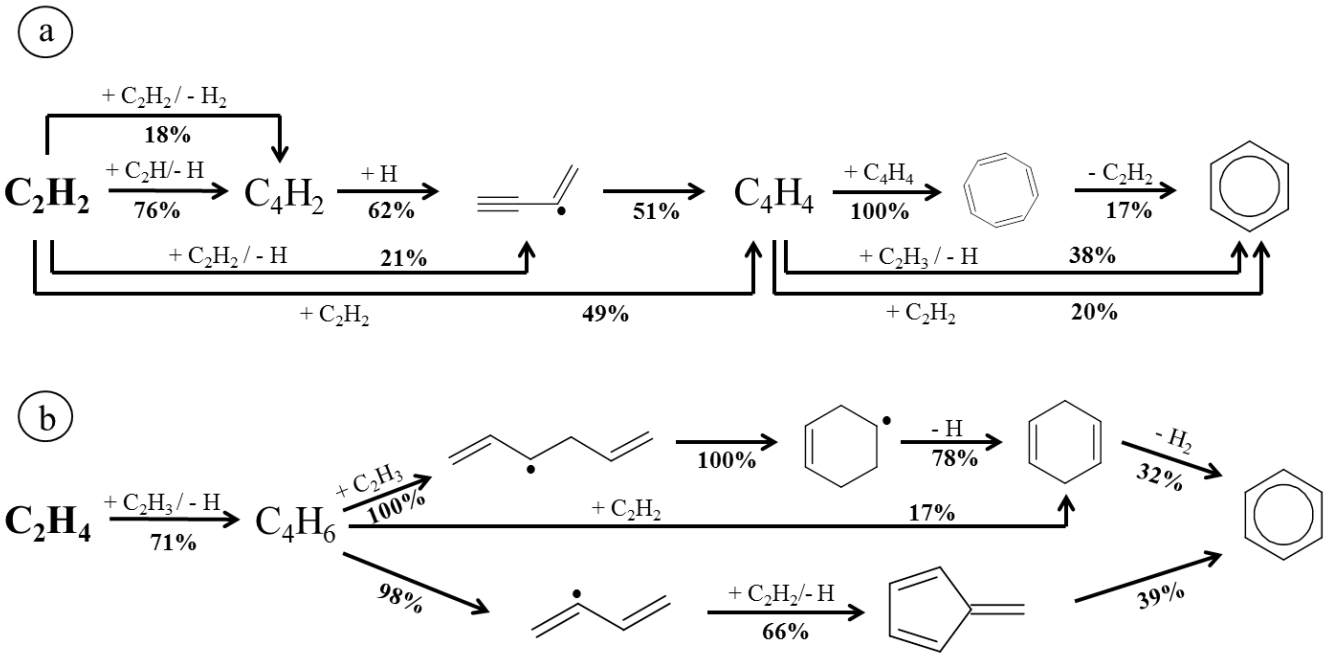

Figure 8: Main reaction pathways for benzene formation at 1173 K, 8 kPa and 1 s of residence time during: a) acetylene pyrolysis; b) ethylene pyrolysis. Percentages are related to the weight of the reaction in the formation of products.

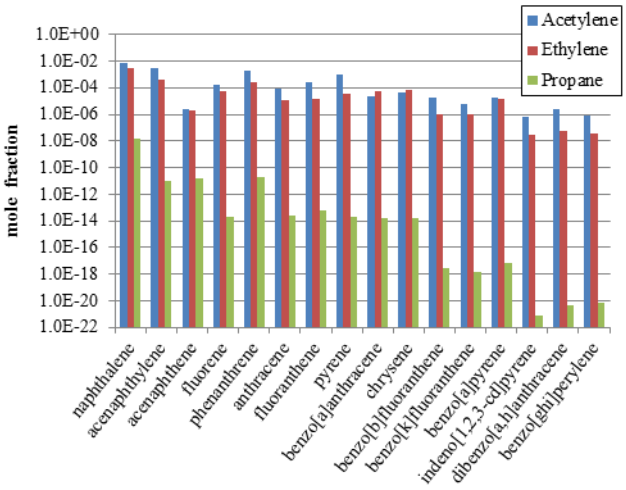

Figure 9: Mole fractions of the EPA-PAHs obtained by modeling during acetylene, ethylene and propane pyrolysis at 1173 K, 15 kPa and a reactant conversion of 50%

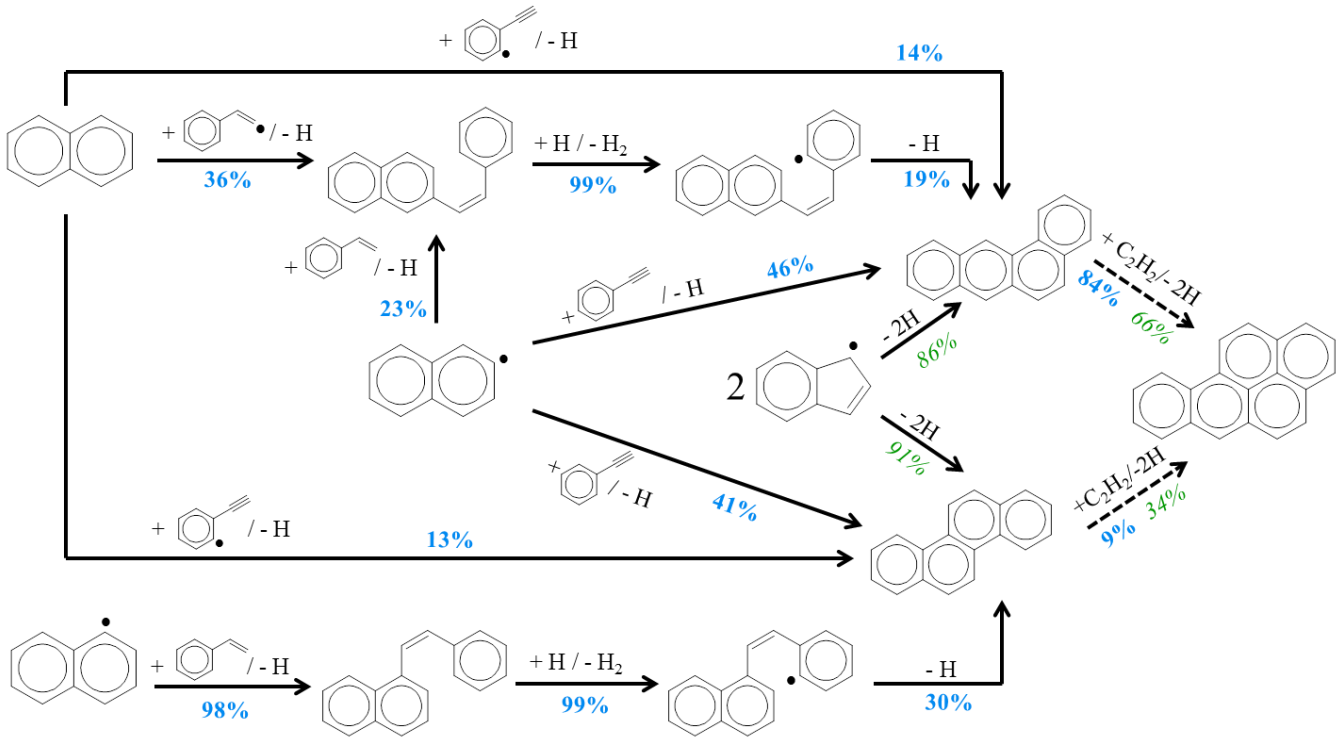

Figure 10: Main reaction pathways for benzo[*a*]pyrene formation at 1173 K, 15 kPa and a reactant conversion of 50% during acetylene pyrolysis (percentages in bold) and ethylene pyrolysis (percentages in italic). Percentages are related to the weight of the reaction in the formation of products. Reaction pathways for naphthalene and indene formation are available in Supplementary data (S6).

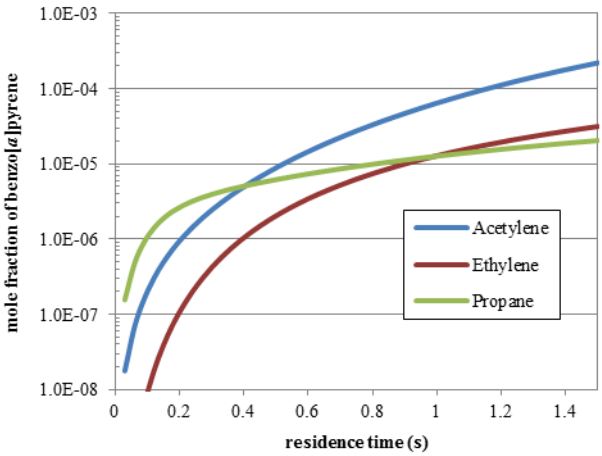

Figure 11: Profiles of benzo[*a*]pyrene mole fraction obtained by modeling during acetylene, ethylene and propane pyrolysis at 1173 K and 15 kPa

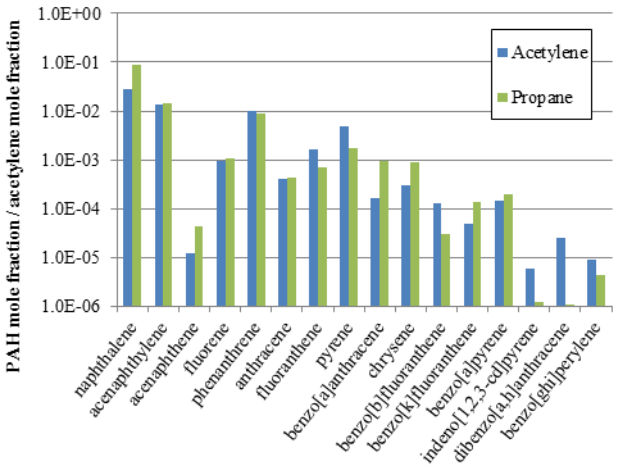

Figure 12: Mole fractions of the EPA-PAHs divided by the mole fraction of acetylene obtained by modeling during acetylene and propane pyrolysis at 1173 K, 15 kPa and a residence time of 1 s